Inorganic Chemistry

Article

pubs.acs.org/IC

Connecting [NiFe]- and [FeFe]-Hydrogenases: Mixed-Valence Nickel–Iron Dithiolates with Rotated Structures

David Schilter,[†] Thomas B. Rauchfuss,*[,†] and Matthias Stein*[,‡]

[†]Department of Chemistry, University of Illinois at Urbana–Champaign, 600 S. Goodwin Avenue, Urbana, Illinois 61801, United States

[‡]Max Planck Institute for Dynamics of Complex Technical Systems, Sandtorstraβe 1, 39106 Magdeburg, Germany

Supporting Information

ABSTRACT: New mixed-valence iron–nickel dithiolates are described that exhibit structures similar to those of mixed-valence diiron dithiolates. The interaction of tricarbonyl salt [(dppe)Ni(pdt)Fe(CO)$_3$]BF$_4$ ([**1**]BF$_4$, where dppe = Ph$_2$PCH$_2$CH$_2$PPh$_2$ and pdt^{2-} = −SCH$_2$CH$_2$CH$_2$S−) with P-donor ligands (L) afforded the substituted derivatives [(dppe)Ni(pdt)Fe(CO)$_2$L]BF$_4$ incorporating L = PHCy$_2$ ([**1a**]BF$_4$), PPh(NEt$_2$)$_2$ ([**1b**]BF$_4$), P(NMe$_2$)$_3$ ([**1c**]BF$_4$), P(*i*-Pr)$_3$ ([**1d**]BF$_4$), and PCy$_3$ ([**1e**]BF$_4$). The related precursor [(dcpe)Ni(pdt)Fe(CO)$_3$]BF$_4$ ([**2**]BF$_4$, where dcpe = Cy$_2$PCH$_2$CH$_2$PCy$_2$) gave the more electron-rich family of compounds [(dcpe)Ni(pdt)Fe(CO)$_2$L]BF$_4$ for L = PPh$_2$(2-pyridyl) ([**2a**]BF$_4$), PPh$_3$ ([**2b**]BF$_4$), and PCy$_3$ ([**2c**]BF$_4$). For bulky and strongly basic monophosphorus ligands, the salts feature distorted coordination geometries at iron: crystallographic analyses of [**1e**]BF$_4$ and [**2c**]BF$_4$ showed that they adopt "rotated" Fe^{I} centers, in which PCy$_3$ occupies a basal site and one CO ligand partially bridges the Ni and Fe centers. Like the undistorted mixed-valence derivatives, members of the new class of complexes are described as Ni^{II}Fe^{I} (S = $^1/_2$) systems according to electron paramagnetic resonance spectroscopy, although with attenuated ^{31}P hyperfine interactions. Density functional theory calculations using the BP86, B3LYP, and PBE0 exchange-correlation functionals agree with the structural and spectroscopic data, suggesting that the spin for [**1e**]$^+$ is mostly localized in a Fe^{I}-centered d(z^2) orbital, orthogonal to the Fe–P bond. The PCy$_3$ complexes, rare examples of species featuring "rotated" Fe centers, both structurally and spectroscopically incorporate features from homobimetallic mixed-valence diiron dithiolates. Also, when the NiS$_2$Fe core of the [NiFe]-hydrogenase active site is reproduced, the "hybrid models" incorporate key features of the two major classes of hydrogenase. Furthermore, cyclic voltammetry experiments suggest that the highly basic phosphine ligands enable a second oxidation corresponding to the couple [(dxpe)Ni(pdt)Fe(CO)$_2$L]$^{+/2+}$. The resulting unsaturated 32e$^-$ dications represent the closest approach to modeling the highly electrophilic Ni–SI$_a$ state. In the case of L = PPh$_2$ (2-pyridyl), chelation of this ligand accompanies the second oxidation.

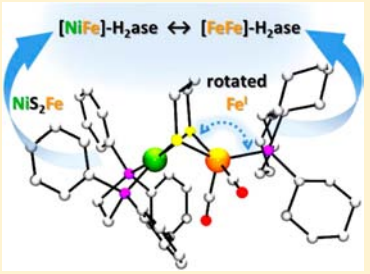

INTRODUCTION

The hydrogenase (H$_2$ase) enzymes catalyze the processing of hydrogen, a reaction that is biologically significant and scientifically topical. These enzymes are prominent in anaerobic bacteria and archaea and are classified according to the metals present at their active sites.[1] In particular, the redox reaction 2H$^+$ + 2e$^-$ ⇌ H$_2$ is mediated by the [FeFe]- and [NiFe]-H$_2$ases, the two major classes of H$_2$ase. Members of a third class, labeled the [Fe]-H$_2$ases, have been characterized but do not perform redox reactions on H$_2$ or protons.[2]

Although no phylogenic relationship exists between the [FeFe]- and [NiFe]-H$_2$ases,[3] their active sites share a number of structural commonalities. Central to their function, the [FeFe]-H$_2$ase enzymes (45–130 kDa) feature an active-site ensemble, the "H-cluster", composed of a binuclear low-spin [Fe$_2$S$_2$] core linked through a cysteinate residue to a [Fe$_4$S$_4$] redox cofactor (Figure 1a).[4,5] Within the [Fe$_2$S$_2$] fragment, the two Fe centers are bridged by a 2-aza-1,3-propanedithiolate cofactor and are further bound to CO and CN$^-$ ligands. The latter participate in hydrogen bonding to neighboring proline, lysine, and serine residues, and thus, while the [Fe$_2$S$_2$] fragment appears only loosely anchored to the backbone, the conformational freedom of the iron coordination spheres is, nevertheless, restricted.

In enzymes isolated in the H$_{ox}$ (Fe^{II}Fe^{I}) state, the proximal (cysteinate-bound) Fe center interacts with a CO ligand that is shared with the other (distal) Fe atom.[6] The latter center, believed to exist in the +I oxidation state, adopts a coordination geometry exposing a vacant site for H$_2$ binding. The "rotated" arrangement of ligands around the distal Fe center results in it being preorganized for catalysis, which likely contributes to the high rates (and low overpotentials) associated with its function. "Rotation" is also observed in [Fe]-H$_2$ase active sites, with Striebitz and Reiher having highlighted the structural and electronic similarities between the two classes of H$_2$ases.[7]

The heterodimeric [NiFe]-H$_2$ases each consist of a small and a large subunit (28 + 60 kDa). These more prevalent enzymes are typically located in the periplasm[10] and feature heterometallic active sites not dissimilar to those of the

Received: May 4, 2012
Published: July 27, 2012

 © 2012 American Chemical Society dx.doi.org/10.1021/ic300910r | Inorg. Chem. 2012, 51, 8931–8941

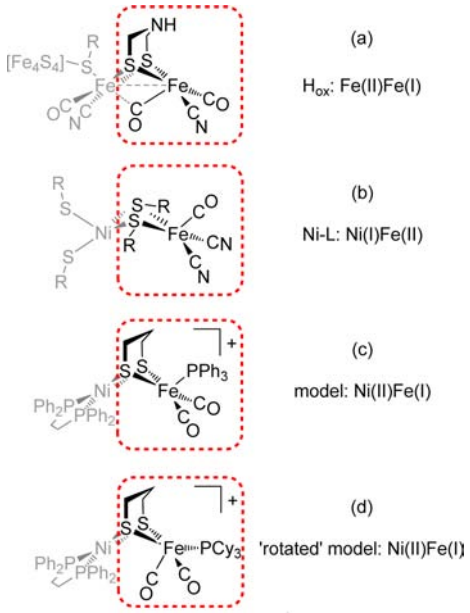

Figure 1. Line drawings of (a) the [FeFe]-H_2ase active site,[6] (b) the [NiFe]-H_2ase active site,[8] (c) a mixed-valence NiFe model complex,[9] and (d) a "rotated" NiFe model complex described in this work. RS^- = cysteinate.

homobimetallic [FeFe]-H_2ases. The [NiFe]-H_2ases also feature a thiolate-bound Fe fragment, in this case linked to a Ni center (Figure 1b). This center exists in a conformationally rigid seesaw geometry, coordinated to four soft, strongly σ- and π-donating cysteinate ligands. These S-donors stabilize Ni in high (+III), intermediate (+II), and low (+I) oxidation states. The states of the [NiFe]-H_2ase enzyme differ not only with respect to the oxidation state of Ni but also with the presence or absence of hydride (and oxygenic) ligands *bridging* the two metals, as well as possibly the degree of protonation of the terminal thiolate ligands (Scheme 1).[11,12]

Scheme 1

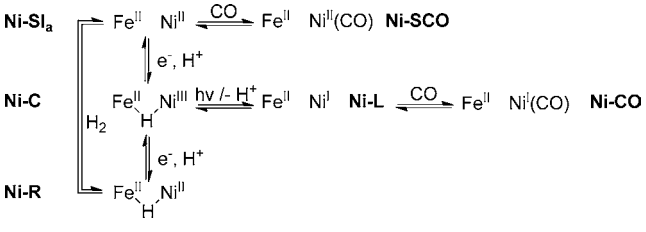

Mixed-valence states play a prominent role in the functioning of both H_2ases. In the [NiFe]-H_2ases, the electron paramagnetic resonance (EPR)-active Ni–C state, an intermediate in the oxidation of H_2, features $Ni^{III}Fe^{II}$ metal centers bridged by a hydride ligand.[13] Proton loss effected by low-temperature UV irradiation of Ni–C results in another $S = {}^1/_2$ state, Ni–L, which features a $Ni^{I}Fe^{II}$ core.[8] In this case, the oxidation states have been assigned according to EPR data (vide infra) and parallels can be drawn between this system (in which the spin resides on Ni) and the H_{ox} state of the [FeFe]-H_2ases (in which the spin resides on the distal Fe). Despite its low formal oxidation state, the Fe^{I} center in the latter is able to activate H_2,[7] by a mechanism that likely involves proton-coupled electron transfer.[14] In contrast, while Ni–L binds CO, it is insufficiently electrophilic to activate H_2. Instead, activation of the H_2 substrate requires the more oxidized Ni–SI_a state, featuring an EPR-silent 32e$^-$ $Ni^{II}Fe^{II}$ core, in which the electrophilic centers are poised to accept a bridging H^- ligand. CO is a potent inhibitor of Ni–SI_a, which is poisoned to afford the active-site adduct $(CO)(cysteinate)_2Ni(\mu\text{-cysteinate})_2Fe(CO)(CN)_2$, known as Ni-SCO.[15] In comparison to the [FeFe]-H_2ases, one can conclude that the [NiFe] enzymes operate with metal centers at higher formal oxidation states, a fact that might be attributed to the four basic cysteinate residues present at the active site.

Synthetic modeling of H_2ase active sites can provide insight into the mechanisms by which these enzymes operate.[16] For example, recent work on the [FeFe]-H_2ases has highlighted the acid/base[17] and redox[14] functionality necessary for catalytic activity. Models for the paramagnetic states are of particular interest, owing to the novelty and synthetic challenges associated with open-shell organometallic compounds. A prominent mixed-valence model is $[(IMes)(CO)_2Fe(pdt)Fe(CO)_2PMe_3]^+$ (Figure 2, left),[18] in which strongly σ-donating

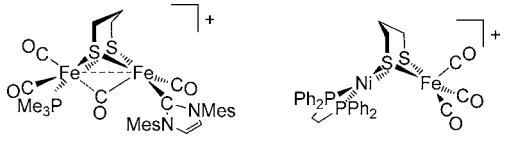

Figure 2. Mixed-valence H_2ase models: $[(IMes)(CO)_2Fe(pdt)Fe(CO)_2PMe_3]^+$ (left) and $[(dppe)Ni(pdt)Fe(CO)_3]^+$ (right).

N-heterocyclic carbene (IMes) and trialkylphosphine ligands represent surrogates for the CN^- ligands found in the enzyme. Notably, the $(IMes)(CO)_2Fe^{I}$ fragment features a semibridging CO, with the two terminal ligands oriented in such a way as to expose a vacant coordination site, thereby reproducing the rotated coordination geometry observed for the distal Fe.

The first paramagnetic models for [NiFe]-H_2ase have recently been reported, one example of which is the prototypical $S = {}^1/_2$ species $[(dppe)Ni(pdt)Fe(CO)_3]^+$ (Figure 2, right).[9] EPR studies support the assignment of oxidation states as $Ni^{II}Fe^{I}$, such that the model resembles Ni–L with oxidation states reversed. Density functional theory (DFT) calculations suggest that the spin is largely Fe-centered and that Ni exists in a square-planar coordination geometry, characteristic of a Ni^{II} (d^8) system. The electrophilicity of the Fe^{I} center in these mixed-valence cations is sufficient to allow the replacement of one CO ligand with PPh_3, thereby affording a more electron-rich species (Figure 1c).[9] This complex was also described as $Ni^{II}Fe^{I}$, and evidently the $(CO)_2(PPh_3)$ ligand set is not as donating as the $(CN)_2(CO)$ ligands present in [NiFe]-H_2ase, given that the $Ni^{I}Fe^{II}$ state is possible in the latter case.

This paper details the synthesis of new $Ni^{II}Fe^{I}$ complexes of the type $[(dxpe)Ni(pdt)Fe(CO)_2L]^+$ (dxpe = dppe or dcpe), characterized spectroscopically, crystallographically, electrochemically, and computationally. Through systematic modulation of the steric bulk and basicity of the mono- and diphosphine (L and dxpe, respectively), new insights are afforded into the relationship between the structure and spectroscopy of mixed-valence derivatives. While our previous report only disclosed compounds in which L is poorly basic,[9] presented here are examples incorporating highly basic ligands L, which differ structurally and spectroscopically. In particular, remarkable changes in the iron coordination geometry are effected, resulting in rare examples of highly distorted iron(I)

dx.doi.org/10.1021/ic300910r | *Inorg. Chem.* 2012, 51, 8931–8941

species, as previewed in Figure 1d and discussed below. Studies on the oxidation of these models to 32e$^-$ $Ni^{II}Fe^{II}$ derivatives afford evidence for the first models for Ni–SI_a, featuring 16e$^-$ Fe^{II} centers.

Herein, we extend the comparison between [FeFe]- and [NiFe]-H_2ases and their model complexes. As we show, the connections between the two classes of H_2ase and their models run much deeper than simple consideration of their coordination spheres. Indeed, the relationships between the two enzymes and their models are also electronic in nature. The new complexes described below serve to exemplify this with respect to the mixed-valence active sites present in the 33e$^-$ H_{ox} and Ni–L states, defining a new link between [FeFe]- and [NiFe]-H_2ases.

RESULTS AND ANALYSIS

Syntheses. In this work, a range of new derivatives of the type [(dxpe)Ni(pdt)Fe(CO)$_2$L]BF_4 (vide supra) were prepared with an emphasis on highly basic phosphines. It was reasoned that highly basic alkylphosphines would lower the $Fe^{I/II}$ couple relative to the $Ni^{II/I}$ couple. Furthermore, it was anticipated that the new complexes could undergo oxidation to coordinatively unsaturated dicationic models for Ni–SI_a. To this end, modulating the basicity of the nickel-bound diphosphine was also of interest, given that it was also expected to have a significant effect on the electron density at the metal centers. Thus, through systematic variation of the phosphine ligands in complexes of the type [(diphosphine)Ni(pdt)Fe(CO)$_2$(monophosphine)]$^+$, new species were generated. As expected, the first electrochemical studies on complexes of this type indicate correlations between the ligand basicity and redox potentials. The compounds described also differ significantly from [(dppe)Ni(pdt)Fe(CO)$_2$$PPh_3$]$BF_4$ in terms of the structure and spectroscopy. The preparation of these new salts is now outlined.

The dppe derivative [**1**]BF_4 could be converted to the salts [**1a**–**1e**]BF_4, while [**2**]BF_4 served as the precursor for [**2a**–**2c**]BF_4, which feature the more strongly σ-donating dcpe ligand (Scheme 2). Briefly, the addition of *in situ* generated tricarbonyl

Scheme 2

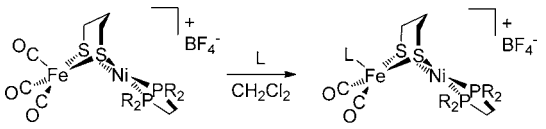

salts to CH_2Cl_2 solutions containing excess monophosphine (L) afforded the substituted radicals. The addition of pentane to the mixtures precipitated yellow to green solids in yields typically exceeding 70%. The products are sensitive to O_2 and H_2O. They decompose to CO-free products at room temperature over the course of days. The salts were characterized according to analytical and electrospray ionization mass spectrometry (ESI-MS) data, with the latter revealing the tendency of the compounds to ionize by loss of BF_4^-, in some cases with dissociation of a CO ligand to afford the ions [(dxpe)Ni(pdt)Fe(CO)$_2$L]$^+$ and [(dxpe)Ni(pdt)Fe(CO)L]$^+$.

Solution IR spectra for the new compounds typically exhibited two ν_{CO} bands (Table 1). However, the $PPh(NEt_2)_2$ derivative [**1b**]BF_4, like the previously reported $PMePh_2$ complex,[9] exhibits four comparably intense bands, assigned to conformers that differ with respect to the disposition of the pdt backbone. The energies of the CO vibrations are affected by the monodentate P-donor ligands, being lowest for complexes of the strong donor PCy_3. For the PCy_3-containing derivatives [**1e**]BF_4 and [**2c**]BF_4, values of ν_{CO} are relatively insensitive to the identity of the nickel-bound diphosphine (dppe vs dcpe). Two ν_{CO} bands lower in energy were observed for the ^{13}CO-labeled complexes [**1d′**]$^+$ and [**1e′**]$^+$.

Table 1. IR Data for New Salts of the Type [(dxpe)Ni(pdt)Fe(CO)$_2$L]BF_4 in CH_2Cl_2 Solution[a]

compound	dxpe	L	ν_{CO}/cm^{-1}
[**1a**]BF_4	dppe	$PHCy_2$	1974, 1914
[**1b**]BF_4	dppe	$PPh(NEt_2)_2$	1982, 1972, 1923, 1903
[**1c**]BF_4	dppe	$P(NMe_2)_3$	1967, 1899
[**1d**]BF_4	dppe	$P(i\text{-}Pr)_3$	1966, 1899
[**1d′**]BF_4[a]	dppe	$P(i\text{-}Pr)_3$	1921, 1857
[**1e**]BF_4	dppe	PCy_3	1966, 1899
[**1e′**]BF_4[a]	dppe	PCy_3	1921, 1856
[**2a**]BF_4	dcpe	PPh_2(2-py)	1988, 1928
[**2b**]BF_4	dcpe	PPh_3	1984, 1925
[**2c**]BF_4	dcpe	PCy_3	1964, 1898

[a]Data for the ^{13}CO-labeled analogues [(dppe)Ni(pdt)Fe(^{13}CO)$_2$L]BF_4 are denoted with prime symbols.

Relation to $S = {}^1/_2$ Hydrides. Although the new complexes contain highly basic ligands and are oxidizable (vide infra), they resist protonation. For example, treatment of the electron-rich complex [**1e**]$^+$ with the strong acid $H(OEt_2)_2BAr^F{}_4$ [$BAr^F{}_4^-$ = $B(3,5\text{-}(CF_3)_2C_6H_3)_4^-$; 1 equiv] resulted in no initial reaction. After 1 h, IR spectroscopic analysis of the reaction solution indicated the presence of [**1e**]$^+$, [**1**]$^+$ (ν_{CO} = 2057 and 1986 cm^{-1}), and [**1**H]$^+$ (ν_{CO} = 2082 and 2024 cm^{-1}). The latter cation was the only CO-containing species detected after 17 h, by which time the solution had changed color from green to deep red. It is interesting to consider the formation of the *tricarbonyl* hydride [**1**H]$^+$; the targeted paramagnetic *dicarbonyl* hydride [**1e**H]$^{2+}$ could not be detected. The treatment of [**1b**]$^+$ with the same acid also afforded [**1**H]$^+$, although in this case the tricarbonyl radical [**1**]$^+$ was the major CO-ligated product. Here it is possible that protonation of the weakly basic amino groups in $PPh(NEt_2)_2$ induces ligand dissociation and CO redistribution. In any case, the cannibalization that leads to the tricarbonyl products suggests that complexes of the present type are not suitable precursors to $S = {}^1/_2$ hydrides and that other synthetic platforms are required to stabilize these Ni–C models.

EPR Spectra for [(dppe)Ni(pdt)Fe(CO)$_2$L]$^+$. All mixed-valence derivatives were characterized by X-band EPR spectroscopy at 110 K; selected spectra were simulated in order to extract g and $A(^{31}P)$ values (Table 2). Spectra not presented here can be found in the Supporting Information (SI).

The EPR spectra of all derivatives prepared feature two overlapping rhombic signals assigned to conformers related by the flipping of the pdt^{2-} chelate ring. The new complexes could be classified into two families, one of which is similar to previously reported species and the other being very distinct. For the triarylphosphine complexes [**2a**]$^+$ and [**2b**]$^+$, each of the resonances is split by a single ^{31}P nucleus (Figures S29 and S32 in the SI), indicating a $Ni^{II}Fe^{I}$ description for these species. Indeed, they are spectroscopically almost identical to their dppe analogues, which were shown by ^{13}CO-labeling studies to adopt

dx.doi.org/10.1021/ic300910r | Inorg. Chem. 2012, 51, 8931–8941

Table 2. EPR Simulation Parameters[a]

compound	g factor	$A(^{31}P)$/MHz	line width/G	weight
[**1a**]BF_4	2.076, 2.046, 2.000	54, 60, 59	9, 13, 7	75
	2.079, 2.039, 2.005	27, 8, 39	8, 6, 9	25
[**1b**]BF_4	2.079, 2.052, 1.997	101, 161, 132	14, 9, 11	52
	2.075, 2.041, 2.002	66, 31, 52	11, 11, 10	48
[**1e**]BF_4	2.089, 2.036, 2.008		6, 4, 10	54
	2.087, 2.036, 2.010		11, 7, 9	46
[**1e′**]BF_4	2.087, 2.036, 2.011		14, 17, 17	54
	2.089, 2.036, 2.007		9, 7, 11	46
Ni–L[8]	2.298, 2.116, 2.043			
H_{ox}[20]	2.097, 2.039, 1.999			
[(IMes)$(CO)_2$Fe(pdt)Fe$(CO)_2PMe_3$]+[18]	2.180, 2.096, 2.052			
[$(PCy_3)(CO)_2$Fe(edt)Fe(CO)dppv]+[21]	2.096, 2.042, 2.001	69, 67, 73		

[a]Each compound has an entry for each of the two isomers, the relative abundances of which are given in the last column. Parameters for [**1e**]BF_4 were derived from both X- and Q-band data. Note: edt = $-SCH_2CH_2S-$.

a structure in which the monophosphine occupies the apical iron coordination site.[9]

Whereas substitution of the diphosphine only subtly influences the Fe center, variation of the iron-bound monophosphine ligand has a marked effect. Motivated by the synthesis of high-fidelity Ni^IFe^{II} (and $Ni^{II}Fe^{II}$) models, strongly donating alkylphosphines were employed because these more basic σ-donors might stabilize the Fe^{II} centers in the targeted complexes. The basic ligands $PHCy_2$, $PPh(NEt_2)_2$, $P(NMe_2)_3$, and $P(i\text{-}Pr)_3$ were incorporated into the complexes [**1a**]$^+$, [**1b**]$^+$, [**1c**]$^+$, and [**1d**]$^+$, respectively, using the general procedure outlined above. Notably, their EPR spectra indicate the ^{31}P hyperfine interactions for these complexes to be greatly attenuated ($A \approx 50$ MHz) relative to triarylphosphine complexes ($A \approx 200$ MHz). Similar values were observed for the "rotated" H_{ox} model [$(PCy_3)(CO)_2$Fe(edt)Fe(CO)-dppv]$^+$,[21] suggesting a connection between the iron(I) coordination geometry and hyperfine interactions. The couplings found here are related to phosphine basicity: they are strongest in the case of $PHCy_2$ and weakest in the complex of $P(i\text{-}Pr)_3$, the most basic of the four P-donor ligands.[22] The influence of the phosphine is clearest for the PCy_3-containing complexes [**1e**]$^+$ and [**2c**]$^+$. In contrast to the complexes of PPh_3 and PPh_2(2-py), which are yellow in color, the PCy_3-containing complexes are deep green (for a representative UV–vis spectrum, see Figure S17 in the SI), suggesting a significant difference in the electronic structure.

Unique among the series of compounds, [**1e**]BF_4 and [**2c**]BF_4 give EPR spectra with *no* ^{31}P hyperfine splitting. The complex [**1e**]$^+$ gives rise to two overlapping rhombic signals at 110 K, the *z* components of which are at lower field (Figure 3); such a pattern is consistent with spin localization on Fe^I. The individual simulated signals, as well as their sum, are presented for X- and Q-band spectra of [**1e**]$^+$ (Figures S21 and S22 in the SI). Lastly, EPR spectroscopy of [**1e**]$^+$ is also distinctive in that a single line was observed at room temperature (see Figure S20 in the SI), whereas all other complexes reported here give spectra reflecting the presence of multiple isomers.

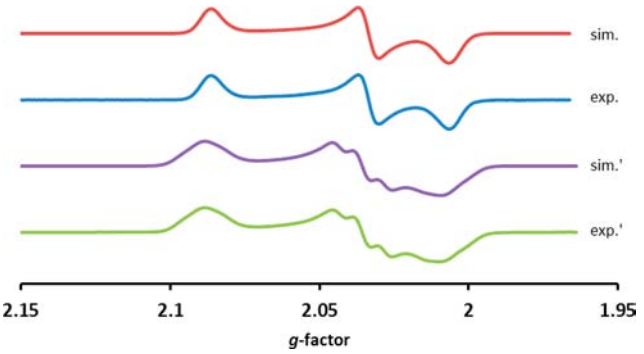

Figure 3. X-band EPR spectra (CH_2Cl_2/PhMe, 110 K) of [**1e**]BF_4 (exp.) and [**1e′**]BF_4 (exp.′). Simulated spectra are also presented.

EPR analysis was also conducted on the ^{13}CO-labeled derivative [**1e′**]$^+$. In a frozen solution, the spectrum features the expected rhombic signals lacking ^{31}P coupling. Furthermore, coupling to the two ^{13}CO ligands is observed, with this being most evident at $g = 2.036$, where the triplet pattern indicates that the CO ligands are equivalent. If the ^{13}CO ligands were indeed basal, the monophosphine ligand would occupy the apical position. However, such a stereochemistry appeared inconsistent with the large $A(^{31}P)$ values that would be expected for apically bound P-donor ligands. The spectral properties were rationalized in terms of the unusual structures adopted by these cations, which are discussed in the following section.

Structure of [(dppe)Ni(pdt)Fe$(CO)_2PCy_3$]BF_4. The structure of the PCy_3 complex salt [**1e**]BF_4 was confirmed crystallographically (Figure 4). Perhaps the most remarkable finding is the distorted geometry of the Fe^I center, which adopts a "rotated" structure. One CO ligand occupies a semibridging position between the Fe and Ni centers, although the Ni–CO distance is long (2.784 Å) and the Fe–C–O atoms are almost collinear (176°).[23] The central methylene of the pdt^{2-} bridge is poised over the vacant Fe coordination site, in contrast to the "unrotated" derivative [(dppe)Ni(pdt)Fe-$(CO)_2PPh_3$]$^+$[9] and the hydride [(dppe)Ni(pdt)HFe-$(CO)_2PPh_3$]$^+$.[24] Unlike the dcpe-containing tricarbonyl [**2**]$^+$, which features a square-pyramidal Fe center,[9] the iron coordination geometry in [**1e**]$^+$ is intermediate between square-pyramidal and trigonal-bipyramidal, with its Addison τ parameter[25] (here the difference between the angles S1–Fe1–C31 and S2–Fe1–P3 divided by 60) being 0.42 ($\tau = 0.02$ for [**2**]$^+$). The mean Fe–C distance in [**2**]$^+$ (1.807 Å) is somewhat greater than that in [**1e**]$^+$ (1.781 Å), owing to the stronger π-back-bonding in the substituted derivative. The coordination environment of Ni is distorted from planarity, with the twist angle between the NiP_2 and NiS_2 planes being 11.6°. The Ni–S (2.213 and 2.224 Å) and Ni–P distances (2.171 and 2.168 Å) are similar to those in [**2**]$^+$. These observations support a +II oxidation state assignment for Ni.

The Ni–Fe distance in [**1e**]$^+$ (2.637 Å) is shorter than that in [**2**]$^+$ (2.818 Å). The reduced intermetallic separation in [**1e**]$^+$ translates to a lower dihedral ("butterfly") angle between the NiS_2 and FeS_2 planes for this species (105.2°) relative to that for [**2**]$^+$ (116.4°). Covalent radii for Ni (1.24 Å) and low-spin Fe (1.32 Å) have been determined from CSD entries,[26] with their sum (2.56 Å) representing an upper limit for the

dx.doi.org/10.1021/ic300910r | Inorg. Chem. 2012, 51, 8931–8941

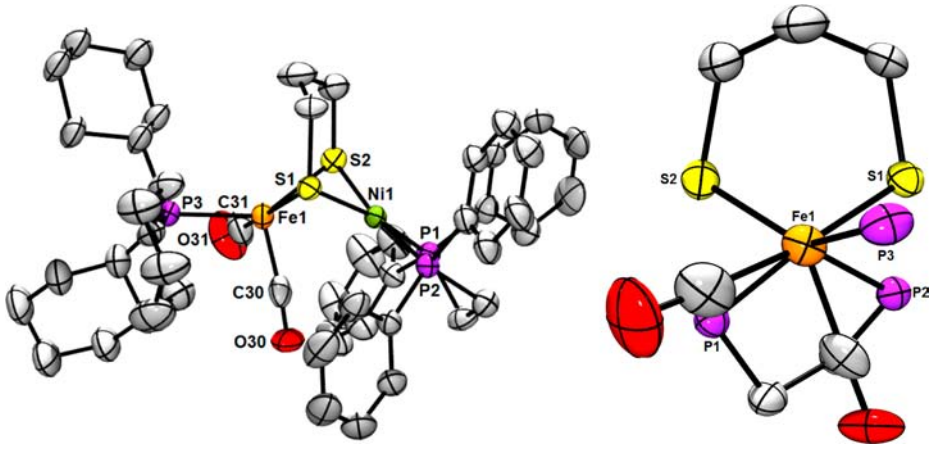

Figure 4. ORTEP of $[\mathbf{1e}]BF_4$ (left) with ellipsoids drawn at the 50% probability level. The H atoms and disordered BF_4^- anion are omitted for clarity. A view down the Fe−Ni vector (right) is also provided, in which the carbocyclic rings are omitted. Selected distances (Å, values calculated using BP/TZVP given in parentheses): Ni1−Fe1, 2.637 (2.77); Ni1−P1, 2.168 (2.23); Ni1−P2, 2.171 (2.23); Ni1−S1, 2.213 (2.28); Ni1−S2, 2.224 (2.25); Fe1−S1, 2.305 (2.36); Fe1−S2, 2.352 (2.33); Fe1−C30, 1.808 (1.78); Fe1−C31, 1.754 (1.76); Fe1−P3, 2.283 (2.36). Selected angles (deg, calculated values in parentheses): Ni1−Fe1−C30, 75.0 (78.4); Fe1−C30−O1, 175.6 (178.3).

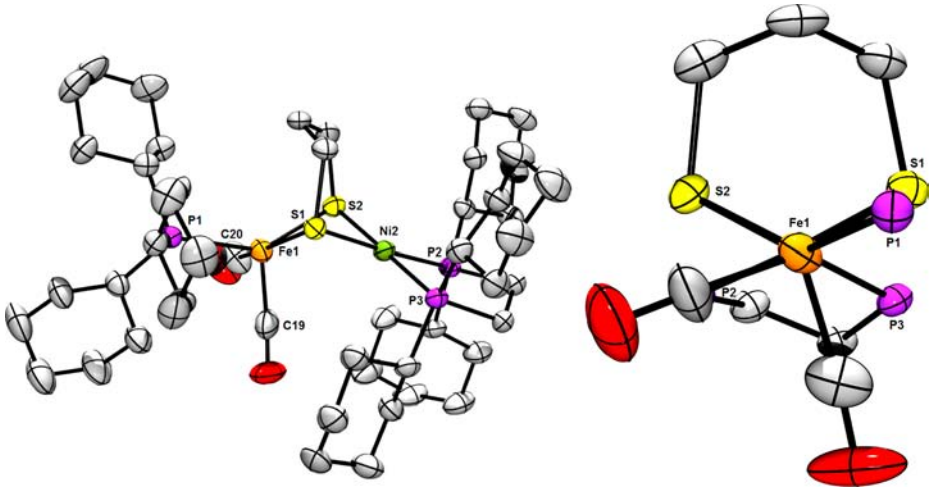

Figure 5. ORTEP of $[\mathbf{2c}]BF_4{\cdot}CH_2Cl_2{\cdot}0.5$pentane (left) with ellipsoids drawn at the 50% probability level. The H atoms, disordered CH_2Cl_2/pentane solvate molecules, and BF_4^- anion are omitted for clarity. A view down the Fe−Ni vector (right) is also provided, in which the carbocyclic rings are omitted. Selected distances (Å): Ni2−Fe1, 2.990; Ni2−P2, 2.192; Ni2−P3, 2.197; Ni2−S1, 2.226; Ni2−S2, 2.231; Fe1−S1, 2.345; Fe1−S2, 2.321; Fe1−C19, 1.781; Fe1−C20, 1.744; Fe1−P3, 2.306. Selected angles (deg): Ni2−Fe1−C19, 84.4; Fe1−C30−O1, 173.4.

length of a formal Ni−Fe bond. Accordingly, such a bond may be considered absent from $[\mathbf{1e}]^+$, although the possibility of weak interactions between these centers is not ruled out. The distance is very similar to that observed crystallographically for [NiFe]-H_2ase (2.60 Å for the Ni−C/Ni−R state in *Desulfovibrio vulgaris* Miyazaki F)[27] and [FeFe]-H_2ase (2.62 Å for the H_{ox} state in *Clostridium pateurianum*),[28] although it is noted that, in the latter case, the Fe centers are within the bonding distance.

Structure of $[(dcpe)Ni(pdt)Fe(CO)_2PCy_3]BF_4$. According to the X-ray crystallographic analysis, the dcpe-containing salt $[\mathbf{2c}]BF_4$ is virtually isostructural with $[\mathbf{1e}]BF_4$ (Figure 5).

Once more, the Fe center exists in a highly distorted square-pyramidal coordination environment (τ = 0.39), although the CO closest to Ni is much further from a bridging position (Ni2−Fe1−C19 = 84°) than is the case with $[\mathbf{1e}]^+$, perhaps suggesting that the present system is more of a "pure" Fe^I system. Moreover, compared to $[\mathbf{1e}]^+$, the nickel coordination geometry in $[\mathbf{2c}]^+$ is closer to square-planar (twist angle between NiP_2 and NiS_2 planes = 2.8°), consistent with a Ni^{II} site. Perhaps owing to the increased basicity of dcpe over dppe, the divalent state for Ni is particularly stabilized for $[\mathbf{2c}]^+$. The large "butterfly" angle (122.5°) reflects the "open" nature of $[\mathbf{2c}]^+$, with the intermetallic separation being significantly greater in this complex (2.990 Å) relative to $[\mathbf{1e}]^+$. It appears that the interactions between the metal centers in $[\mathbf{2c}]^+$ are of a negligible nature, indicative of the strongly donating ligands at Ni satisfying its Lewis acidity such that no further contacts with Fe1 or C19 are necessary.

Cyclic Voltammetry. The effects of the phosphine substituents on the electronic structure of the mixed-valence complexes were probed by cyclic voltammetry. Analysis of selected derivatives in a CH_2Cl_2/NBu_4PF_6 electrolyte solution was performed under a N_2 atmosphere. Well-defined reduction and oxidation waves were observed, with these being assigned to metal-centered events, which on the basis of the peak separations (ΔE_p) involve the transfer of a single electron. For example, in the case of $[\mathbf{2c}]BF_4$, separations of 0.071 and 0.072

dx.doi.org/10.1021/ic300910r | *Inorg. Chem.* 2012, 51, 8931−8941

V were measured for the anodic and cathodic waves, respectively; under these conditions, the value for the ferrocene/ferrocenium (Fc/Fc^+) couple was found to be 0.069 V. Reduction of the $Ni^{II}Fe^{I}$ cations afforded neutral $Ni^{I}Fe^{I}$ complexes, with i_{pc}/i_{pa} values being close to unity (Table 3). This reversibility suggests that the neutral species are stable;

Table 3. Redox Potentials (V vs Fc/Fc^+) and Associated Electrochemical Data for $[(dxpe)Ni(pdt)Fe(CO)_2L]BF_4$ (1 mM) in the NBu_4PF_6 Electrolyte (100 mM CH_2Cl_2 Solution) Recorded at 0.1 V s^{-1}[a]

compound	dxpe	L	$E(Ni^{II}Fe^{I}/Ni^{II}Fe^{II})$ ($\lvert i_{pc}/i_{pa}\rvert$, $\lvert\Delta E_p\rvert$)	$E_{1/2}(Ni^{I}Fe^{I}/Ni^{II}Fe^{I})$ ($\lvert i_{pc}/i_{pa}\rvert$, $\lvert\Delta E_p\rvert$)
1[29]	dppe	CO	−0.04 (irrev.)	−0.58 (1.08)
	dppe	PPh_2(2-py)	−0.19 (irrev.)	−0.83 (1.00, 0.072)
	dppe	PPh_3	−0.04 (0.51, 0.068)	−0.80 (0.99, 0.062)
$[\mathbf{1e}]BF_4$	dppe	PCy_3	−0.14 (0.68, 0.076)	−0.92 (1.00, 0.072)
2[29]	dcpe	CO	0.22 (irrev.)	−0.82 (1.05)
$[\mathbf{2a}]BF_4$	dcpe	PPh_2(2-py)	−0.29 (irrev.)	−1.11 (1.10, 0.067)
$[\mathbf{2b}BF_4$	dcpe	PPh_3	−0.01 (0.52, 0.063)	−1.11 (1.09, 0.073)
$[\mathbf{2c}]BF_4$	dcpe	PCy_3	−0.12 (0.97, 0.071)	−1.21 (1.09, 0.072)

[a]Oxidations are given as half-wave potentials and anodic peak potentials for partially reversible and irreversible couples, respectively. Measurements for $(dxpe)Ni(pdt)Fe(CO)_3$ were recorded on PhCN solutions.

indeed, in addition to the robust tricarbonyl complexes **1** and **2** used as precursors in the present study, the substituted $Ni^{I}Fe^{I}$ derivative $(dppe)Ni(pdt)Fe(CO)_2(PPh_3)$ has also been isolated as a stable solid.[24] Consistent with the reduction being Ni-centered, use of the more basic dcpe ligand in place of dppe caused, in most cases, a cathodic shift on the order of 0.3 V for the couple $[(dxpe)Ni(pdt)Fe(CO)_2L]^{0/+}$. Similar shifts have been reported for the couples $[(dxpe)Ni(edt)Fe(CO)_3]^{0/+}$ and $[(dxpe)Ni(pdt)Fe(CO)_3]^{0/+}$ when the diphosphine is changed.[29]

The anodic waves observed for the mixed-valence salts are assigned to Fe-centered oxidations, generating dicationic $Ni^{II}Fe^{II}$ complexes. In contrast to the reductions, oxidations are virtually unaffected by the identity of the nickel-bound diphosphine, dppe vs dcpe, despite strong differences in their basicities.[30] Complementarily, the diphosphine also has little influence on the ν_{CO} values of the mixed valence compounds (vide supra), further confirming the assignment of the anodic waves. The $[(dxpe)Ni(pdt)Fe(CO)_2L]^{+/2+}$ couple is sensitive to the Fe coordination sphere. For example, substitution of PPh_3 in $[\mathbf{2b}]BF_4$ for the stronger σ-donor PCy_3 ($[\mathbf{2c}]BF_4$) results in a cathodic shift of 0.11 V. The latter compound, decorated with three alkylphosphines, exhibits the mildest (and most reversible) oxidations. Replacement of the N_2 atmosphere with H_2 did not affect any of the results described.

The anodic waves observed for the PPh_2(2-py) species $[(dppe)Ni(pdt)Fe(CO)_2PPh_2(2\text{-}py)]^+$ and $[(dcpe)Ni(pdt)Fe(CO)_2PPh_2(2\text{-}py)]^+$ ($[\mathbf{2a}]^+$) were considerably different from those for other substituted derivatives. While voltammograms of the dppe complex are complicated, $[\mathbf{2a}]^+$ exhibits more well-defined behavior. In such cases, the electrophilic Fe^{II} centers generated upon oxidation are thought to bind the pyridyl groups such that complexes of the type $[(diphosphine)Ni(pdt)Fe(CO)_2(\kappa_2\text{-}PPh_2(2\text{-}py))]^{2+}$ form. Thus, chelation occurs to "quench" the Lewis acidic Fe site by completing its octahedral coordination sphere. The process is very rapid, and the irreversibility of the oxidation waves even at high scan rates (1 V s^{-1}) precluded extraction of kinetic data. Representative data are given for $[\mathbf{2a}]BF_4$ and $[\mathbf{2c}]BF_4$ (Figure 6), and further electrochemical data can be found in the SI.

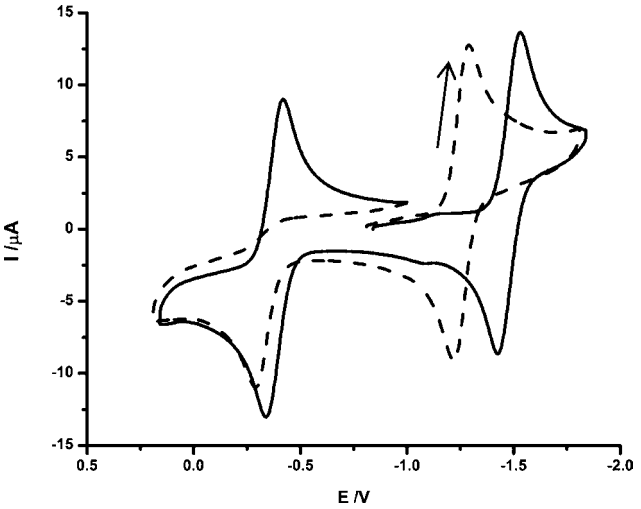

Figure 6. Cyclic voltammograms for the PPh_2(2-py) derivative $[\mathbf{2a}]BF_4$ (dotted trace) and PCy_3 derivative $[\mathbf{2c}]BF_4$ (solid trace).

Reactivity. The irreversibility of the $[\mathbf{1}]^{+/2+}$ couple suggested that the electrophilicity of the tricarbonyl cations might result in enhanced reactivity. Indeed, the treatment of **1** with $FcBF_4$ (2 equiv) in CH_2Cl_2 afforded a complex mixture including the fluoride complex $[(dppe)Ni(pdt)FFe(CO)_3]^+$ ($[\mathbf{1F}]^+$), identified according to IR and MS data. The same fluoride complex was generated by treating **1** with 1-fluoropyridinium tetrafluoroborate (1 equiv) in CH_2Cl_2/MeCN (ν_{CO} = 2114, 2067, and 2028 cm^{-1}; m/z 733.7 $[\mathbf{1F} - CO + MeCN]^+$, 720.7 $[\mathbf{1F}]^+$; Figures S38 and S39 in the SI).

The observation of F^- abstraction suggested the use of the noncoordinating anion $BAr^F{}_4^-$, whose Fc^+ salt allows for clean conversion of **1** to $[\mathbf{1}]BAr^F{}_4$.[9] A mixture containing $[\mathbf{1}]BAr^F{}_4$ and excess $FcBAr^F{}_4$ was used in preliminary hydride abstraction experiments. No reactivity was observed when the solution was exposed to H_2, even in the presence of the (noncoordinating) external base P(*o*-tolyl)$_3$. However, the targeted hydride $[\mathbf{1H}]^+$ was observed when the stronger hydride source Ph_2SiH_2 was employed. Thus, the treatment of a CH_2Cl_2 solution of $[\mathbf{1}]BAr^F{}_4$ and $FcBAr^F{}_4$ (1 equiv) with Ph_2SiH_2 (10 equiv) resulted in complete conversion to $[\mathbf{1H}]^+$ after 4 h, as evidenced by IR (Figures S40 and S41 in the SI) and ESI-MS measurements. An analogous experiment, in which $[\mathbf{1}]BAr^F{}_4$ alone was allowed to interact with Ph_2SiH_2, afforded some $[\mathbf{1H}]^+$, although in this case, the reaction was slower and several unidentified coproducts were observed by IR spectroscopy (Figure S42 in the SI). A possible mechanism for the reaction involves the binding of Ph_2SiH_2 to $[\mathbf{1}]^+$, followed by oxidation and heterolytic Si−H bond cleavage. Nevertheless, other pathways are also possible, especially given the propensity of Ph_2SiH_2 to participate in H-atom-transfer reactions.[31,32]

DFT Calculations. DFT calculations were performed for the "rotated" complex $[\mathbf{1e}]^+$ in an effort to rationalize EPR data and assign the oxidation states. The calculations support a $Ni^{II}Fe^{I}$ description, with the predicted structural parameters agreeing with those determined experimentally to within 0.1 Å

dx.doi.org/10.1021/ic300910r | Inorg. Chem. 2012, 51, 8931−8941

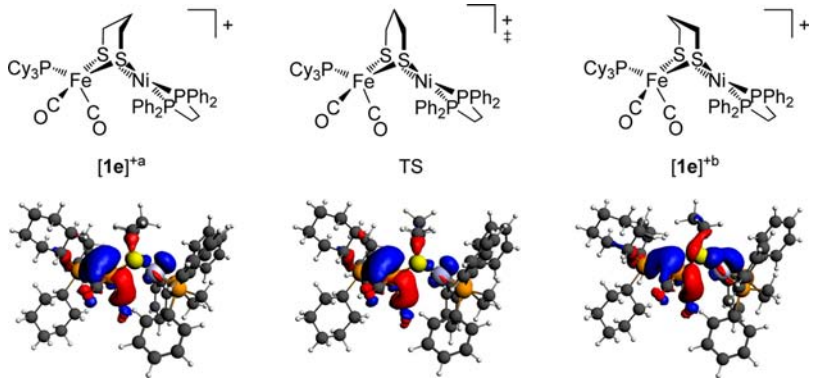

Figure 7. Schematic drawings of the $[\mathbf{1e}]^{+}$ conformations and the TS between the two. Below these are isocontour plots of the SOMO at an isocontour value of 0.03 a.u. for $[\mathbf{1e}]^{+a}$, TS, and $[\mathbf{1e}]^{+b}$.

for bond lengths and 3° for bond angles (Figure 4 caption, vide supra). As was described above, the flipping of the pdt^{2-} chelate ring gives rise to two conformers, which differ in the relative orientation of the central $-CH_2-$ group. These "flipamers" are referred to as "a" or "b" depending on whether this group is pointing to the Ni or Fe atoms, respectively. Optimized structures for the flipamers $[\mathbf{1e}]^{+a}$ and $[\mathbf{1e}]^{+b}$ (the conformer found in the solid state) were determined. The transition state (TS) for their interconversion was also characterized; chemical structures and isocontour plots of the singly occupied molecular orbital (SOMO) are presented in Figure 7.

The Ni−Fe−P angles in $[\mathbf{1e}]^{+a}$ and $[\mathbf{1e}]^{+b}$ are 152° and 158°, respectively, with the PCy_3 ligand being displaced from an ideal "apical" position. In each case, one CO ligand is semibridging, with the CO−Ni distances in $[\mathbf{1e}]^{+a}$ and $[\mathbf{1e}]^{+b}$ being 3.58 and 3.39 Å, respectively. In the TS, which is characterized by a single imaginary frequency corresponding to chelate ring inversion, the pdt^{2-} ligand is planar and perpendicular to the Ni−Fe vector. The ring flip has a significant effect on the Ni−Fe distance, which increases from 2.87 Å in $[\mathbf{1e}]^{+a}$ to 3.00 Å in the TS, before decreasing to 2.77 Å in $[\mathbf{1e}]^{+b}$. A further conformer ($[\mathbf{1e}]^{+a'}$) was analyzed, with it being similar in structure to $[\mathbf{1e}]^{+a}$ but with PCy_3 occupying a basal site (Figure S24 in the SI). This stereochemistry is of particular relevance to the enzyme, in which the strongly σ-donating CN^- ligands are basal. Selected metrics for the optimized structures are given in Table S1 in the SI.

The two flipamers of $[\mathbf{1e}]^{+}$ are closely matched in energy, yet they have a large barrier to interconversion (Table 4). Given the steric demand of the apical PCy_3 ligand, it was expected that flipamer "a" is more stable than "b". Indeed, all DFT calculations suggest that the Gibbs free energy of $[\mathbf{1e}]^{+a}$ is lower by 2−4 kcal mol^{-1}. The activation barrier for conversion of $[\mathbf{1e}]^{+a}$ to $[\mathbf{1e}]^{+b}$ is 6−9 kcal mol^{-1}. The calculated barrier is only slightly affected when van der Waals interactions are considered, with BP/TZVP and BP86+VDW/TZVP calculations giving 7.6 and 5.8 kcal mol^{-1}, respectively. The hybrid functionals B3LYP and B3LYP+VDW/TZVP predicted barriers of 8.6 and 9.0 kcal mol^{-1}, respectively.

Table 4. Changes in the Gibbs Free Energy (kcal mol^{-1}) for the (i) Ring-Flipping Process between $[\mathbf{1e}]^{+a}$ and $[\mathbf{1e}]^{+b}$ and (ii) Turnstile Rotation Interconverting $[\mathbf{1e}]^{+a}$ and $[\mathbf{1e}]^{+a'}$

functional/basis set	$\Delta G_{a\rightarrow b}$	$\Delta G_{a\rightarrow TS}$	$\Delta G_{TS\rightarrow b}$	$\Delta G_{a\rightarrow a'}$
BP/TZVP	+2.5	+7.6	−5.1	−0.2
BP+D/TZVP	+1.4	+5.8	−4.4	+1.1
B3LYP/TZVP	+2.4	+8.6	−6.2	+0.5
B3LYP+D/TZVP	+4.2	+9.0	−4.8	+0.9

Despite the steric bulk of PCy_3, the calculations indicate that this ligand, not CO, is slightly favored to occupy the pseudoapical Fe site. Indeed, the turnstile rotation process converting $[\mathbf{1e}]^{+a}$ (pseudoapical PCy_3) to $[\mathbf{1e}]^{+a'}$ (basal PCy_3) is calculated to be endergonic by about 1 kcal mol^{-1} (Table 4) when dispersion corrections are considered. Similar results were obtained when a COSMO model was employed to simulate interactions with a CH_2Cl_2 solvent (data not shown).

Theory (BP/TZVP) indicates that the unpaired spin for $[\mathbf{1e}]^{+}$ resides almost exclusively on the Fe center, irrespective of which conformation the complex adopts (Table 5). As is evident in the isocontour plots for the $[\mathbf{1e}]^{+}$ conformers (Figure 7), pdt^{2-} chelate ring flipping or Fe turnstile rotation have little influence on the spin density distribution. Similar results were obtained from spin-unrestricted calculations (values obtained using B3LYP/TZVP can be found in Table S2 in the SI).

Table 5. Atomic Spin Populations for the Conformers of $[\mathbf{1e}]^{+}$ Calculated Using BP/TZVP

conformer	ρ(Fe)	ρ(Ni)	$\rho(P_{dppe})$	$\rho(PCy_3)$
$[\mathbf{1e}]^{+a}$	0.94	0.03	0.01, 0.01	0.007
TS	0.94	0.02	0.01, 0.01	−0.01
$[\mathbf{1e}]^{+b}$	0.87	0.07	0.01, 0.01	0.03
$[\mathbf{1e}]^{+a'}$	0.79	0.05	0.01, 0.01	−0.02

Despite the spin distributions in $[\mathbf{1e}]^{+a}$ and $[\mathbf{1e}]^{+b}$ being almost identical, their isotropic ^{31}P hyperfine interactions (+10 and +72 MHz, respectively) differ somewhat, which might be expected given the increase in unpaired spin density $\rho(PCy_3)$ from 0.007 for $[\mathbf{1e}]^{+a}$ to 0.03 for $[\mathbf{1e}]^{+b}$ (BP86/TZVP). Nevertheless, the magnitudes of these $A(^{31}P)$ values are low, and they could not be resolved in the experimental EPR spectra. The extremely weak nature of the hyperfine interactions is proposed to result from the unusual geometry of $[\mathbf{1e}]^{+}$ because similar DFT calculations for the "unrotated" analogue $[(dppe)Ni(pdt)Fe(CO)_2PPh_3]^{+}$ (in which the triphenylphosphine occupies an axial position) predicted much larger isotropic hyperfine interactions (+178 and +204 MHz).[9]

The **g**-tensor principal values were calculated from spin-unrestricted coupled-perturbed self-consistent-field (CP-SCF) and spin-restricted zeroth-order regular approximation

dx.doi.org/10.1021/ic300910r | Inorg. Chem. 2012, 51, 8931−8941

(ZORA) calculations (Table S3 in the SI). The BP86 functional was found to underestimate g shifts, while PBE0 overestimated g shifts; the best agreement was obtained using the B3LYP hybrid functional in spin-unrestricted calculations. The SCF consideration of spin−orbit coupling in spin-restricted calculations with Slater basis functions gave larger g shifts compared to the effective potential approach through the CP-SCF equation. All methods afforded rhombic **g** tensors for the various isomers of $[\mathbf{1e}]^+$ (Table S2 in the SI), with the smallest g component, g_3, being close to g_e. This is suggestive of a $d(z^2)$-centered SOMO; pure nickel(I) species can be ruled out because larger g shifts would be expected in such a case, owing to the significant $d(x^2-y^2)$ character of the SOMO in a low-spin d^9 square-planar system. In contrast, the g values reported for Ni−L (2.298, 2.116, and 2.043),[19] in particular the deviation of the g_z component from g_e (2.0023), are indicative of the presence of Ni^I in this state of the enzyme.

DISCUSSION

The [FeFe]- and [NiFe]-H_2ases, in their H_{ox} and Ni−L states, respectively, share several key features. Aside from their similar coordination spheres, the binuclear active sites are both EPR-active, with the $33e^-$ clusters existing in low-spin ($S = {}^1/_2$) configurations. However, while the spin in H_{ox} is located on the rotated Fe^I site, in Ni−L it resides on the Ni center. In the latter case, Fe is in the +II oxidation state and DFT calculations suggest that it does not adopt a rotated structure.[19] This difference is unsurprising given that a vacant Fe coordination site is necessary for H_{ox} to bind H_2,[7] whereas the [NiFe]-H_2ases (in the Ni−SI_a state) probably activate H_2 by a different mechanism.[31]

The triarylphosphine complexes $[\mathbf{2a}]^+$ and $[\mathbf{2b}]^+$ are spectroscopically similar to the $Ni^{II}Fe^I$ complexes reported earlier[9] in that the ^{31}P nucleus of the monophosphine couples strongly to the Fe^I center. Given that Ni−L has a Ni^IFe^{II} core with strongly donating CN^- ligands at the basal Fe coordination sites, improved models were expected to result from the coordination of highly basic phosphines to the Fe center. It was necessary to employ bulky alkylphosphines because we have found that phosphines that are both basic *and* small [e.g., PMe_3 and P(*n*-Bu)$_3$] trigger disproportionation-type reactions when interacted with $[\mathbf{1}]^+$.[9]

With bulky, basic phosphine ligands, these new $Ni^{II}Fe^I$ complexes, also of formula $[(dxpe)Ni(pdt)Fe(CO)_2L]^+$, differ from those previously described in terms of their structure and spectroscopy. It is proposed that the magnitude of the ^{31}P hyperfine interaction is highly sensitive to the position of the monophosphine ligand and is greatest in the case when L is apically bound, where overlap with the Fe-centered SOMO is maximized. In turn, the position of this ligand is governed by its basicity. Whereas triarylphosphines are bound apically, complexes of more basic ligands such as $PHCy_2$ are thought to be more structurally distorted. This effect, perhaps caused by repulsion between the P lone pair and Fe-centered SOMO, serves to decrease the overlap between the electron in the latter and the ^{31}P nucleus. In the extreme case of PCy_3, complexes featuring a highly distorted $Fe(CO)_2(PR_3)$ site are afforded, for which no hyperfine interactions were observed. Indeed, the smallest Ni−Fe−C angle in $[\mathbf{1e}]^+$ (75°) and, to a lesser extent, that in $[\mathbf{2c}]^+$ (84°) suggest that Fe exists in a "rotated" coordination geometry, a theme prevalent in mixed-valence $Fe^{II}(pdt)Fe^I$ complexes.[17,21] For example, in $[(IMes)(CO)_2Fe(pdt)Fe(CO)_2PMe_3]^+$, the smallest C−Fe−Fe angle is even more acute (57°). It is likely that the "rotated" Fe stereochemistry found for $[\mathbf{1e}]^+$ and $[\mathbf{2c}]^+$ results from the presence of strongly σ-donating ligands, although the large steric profile of the trialkylphosphines employed [cone angles: P(*i*-Pr)$_3$ 160° and PCy_3 170° vs PPh_3 145°][33] may also play a role.

The molecular structure of $[\mathbf{1e}]^+$ calculated by DFT closely matches that obtained by X-ray crystallography. Indeed, both indicate a "rotated" structure for the Fe^I site, with the PCy_3 ligand occupying a pseudoapical position, despite its steric bulk. The calculations also allowed for characterization of the electronic structure, which features a Fe-centered SOMO with substantial $d(z^2)$ character. Importantly, the orbital is roughly orthogonal to the Fe−P bond such that it is unaffected by the $^{31}PCy_3$ nucleus, which accounts for the lack of hyperfine splitting in the experimental EPR spectra. While spectra of the ^{13}CO-labeled complex $[\mathbf{1e'}]^+$ suggested that the ^{13}CO ligands could be equivalent, upon consideration of the X-ray structure, it is likely that the they are in fact inequivalent and give rise to a pseudotriplet due to the $A(^{13}C)$ values being similar in magnitude. For the diiron model $[(IMes)(CO)_2Fe(pdt)Fe(CO)_2PMe_3]^+$, single-point spin-restricted (ROB3LYP) calculations predicted a significant spin density on the rotated Fe center, consistent with its assignment as Fe^I.[34] As is the case with $[\mathbf{1e}]^+$, the SOMO appears to have significant $d(z^2)$ character, as might be expected for a low-spin, square-pyramidal d^7 system.

Despite their heterobimetallic nature, $[\mathbf{1e}]^+$ and $[\mathbf{2c}]^+$ can be considered models for H_{ox}. This state of [FeFe]-H_2ase is thought to adopt a rotated structure to reduce the electronic asymmetry by virtue of the semibridging CO, onto which spin may be delocalized. The rotated $Fe(CO)_2(PCy_3)$ centers in these models structurally mimic the distal $Fe(CN)(CO)_2$ unit present in the [FeFe] enzyme, although the semibridging CO is not within bonding distance of Ni.

The relevance of complexes $[\mathbf{1e}]^+$ and $[\mathbf{2c}]^+$ to H_{ox} is confirmed not only crystallographically but also spectroscopically. As with the triarylphosphine complexes, the g shifts obtained are not dissimilar to those of H_{ox} (Table 2), although the signals are considerably more rhombic. Indeed, the values obtained for the PCy_3 complex $[\mathbf{1e}]^+$ (2.089, 2.036, and 2.008), compared to those for $[(dppe)Ni(pdt)Fe(CO)_2PPh_3]^+$ (2.066, 2.036, and 2.006),[9] indicate significant g strain and movement away from idealized C_s symmetry (i.e., by "rotation") in the former case. The lack of ^{31}P hyperfine coupling in these "rotated" models is consistent with the DFT calculations in that of the SOMO is oriented toward a vacant coordination site, as it is in H_{ox}.

The description of new derivatives as $Ni^{II}Fe^I$ complexes is further corroborated upon consideration of the effects of phosphine substitution on their electrochemical properties. Variation of the diphosphine greatly alters the $[(dxpe)Ni(pdt)Fe(CO)_2L]^{0/+}$ couple, whereas the $[(dxpe)Ni(pdt)Fe(CO)_2L]^{+/2+}$ couple is more strongly affected by the monophosphine L. Thus, the data are consistent with the oxidations $Ni^IFe^I \rightarrow Ni^{II}Fe^I \rightarrow Ni^{II}Fe^{II}$. A key finding is that oxidation to afford $Ni^{II}Fe^{II}$ species can be reversible and occurs at relatively mild potentials. In contrast to the substituted derivatives, the tricarbonyl dications are unstable, as evidenced by the irreversibility of the couples $[\mathbf{1}]^{+/2+}$ and $[\mathbf{2}]^{+/2+}$.[29] These results emphasize the role of terminal ligands on the Fe electronic structure and are significant in that the electrochemically generated substituted dications represent the closest approaches to the diamagnetic $32e^-$ Ni−SI_a state of [NiFe]-

dx.doi.org/10.1021/ic300910r | Inorg. Chem. 2012, 51, 8931−8941

H_2ase. Indeed, these models have highly electrophilic $Ni^{II}Fe^{II}$ cores, a key feature that allows for the heterolytic activation of H_2 in nature. Moreover, dicationic models bearing five-coordinate Fe centers would differ from previously reported nickel(II)−iron(II) dithiolates, in which this center is coordinatively saturated.[35,36]

SUMMARY

New examples of mixed-valence ($S = {}^1/_2$) nickel−iron dithiolates of the formula [(diphosphine)Ni(dithiolate)Fe$(CO)_2$L]$^+$ have been prepared and fully characterized. Their unambiguous description as $Ni^{II}Fe^{I}$ species, achieved experimentally and by DFT, contrasts the $Ni^{I}Fe^{II}$ core present in the Ni−L state of [NiFe]-H_2ase. However, the new Fe-centered radicals ("inverse" Ni−L models) bear remarkable similarity to H_{ox}. While weakly basic ligands (L = triarylphosphine) in the mixed-valence complexes occupy the apical Fe site and participate in strong $^{31}P-Fe^{I}$ hyperfine interactions, more basic monophosphines (L = trialkylphosphine) do not give rise to such a coupling. Significantly, structural and DFT studies on complexes in the latter class allow for this to be rationalized in terms of the "rotation" of the Fe fragments. Thus, in these compounds bearing strong σ donors, overlap between the Fe-centered SOMO and the monophosphine is avoided by adoption of the rotated structure. The distortion in the Fe coordination sphere is a key feature of the distal Fe site in the H_{ox} state of [FeFe]-H_2ase. Reproducing the NiS_2Fe core present in the [NiFe]-H_2ases, while also mimicking the spectroscopy and "rotated" structure of the [FeFe]-H_2ases, complexes of the present type represent unprecedented hybrid models, from which new parallels between the different H_2ases can be drawn.

EXPERIMENTAL SECTION

Unless otherwise stated, chemicals were purchased from commercial sources and used as received. Compounds **1**[24] and **2**[29] and $FcBAr^F{}_4$[37] were prepared according to literature methods. All reactions were conducted in an MBraun glovebox equipped with a solvent purification system; the concentrations of O_2 and H_2O in a N_2 atmosphere were less than 1 ppm. The mixed-valence salts were stored at −28 °C. IR spectra of complexes (in CH_2Cl_2) were recorded on a Perkin-Elmer Spectrum 100 FT-IR spectrometer. EPR spectra of complexes (~1 mM in 1:1 CH_2Cl_2/PhMe) were recorded on either a Varian E-line 12″ Century Series X-band or a 15″ Q-band CW spectrometer. ESI-MS data of compounds in CH_2Cl_2 were acquired using a Waters Micromass Quattro II spectrometer. Cyclic voltammetry experiments were carried out in a one-compartment glass cell using a CH Instruments CHI600D electrochemical analyzer. The working, counter, and pseudoreference electrodes were glassy carbon, platinum, and silver, respectively. The analyte (1 mM) and NBu_4PF_6 (100 mM) were dissolved in CH_2Cl_2, and potentials (reported here relative to internal Fc/Fc^+) were swept at 0.1 V s^{-1}. Analytical data were acquired using an Exeter Analytical CE-440 elemental analyzer. UV−vis data were acquired on a Varian Cary 50 Bio spectrophotometer. Crystallographic data were collected using either a Bruker X8 ([**1e**]BF_4) or a Siemens SMART diffractometer ([**2c**]BF_4), each of which was equipped with a Mo Kα source (λ = 0.71073 Å) and an Apex II detector.

Phosphine-Substituted Derivatives ([1a−1e]BF_4 and [2a−2c]BF_4). [(dxpe)Ni(pdt)Fe$(CO)_3$] (20 μmol) and $FcBF_4$ (20 μmol) were dissolved in CH_2Cl_2 (2 mL) with rapid stirring. After 1 min, the solution was added dropwise to the appropriate phosphine (100 μmol) in CH_2Cl_2 (0.5 mL) with stirring. After 0.5 min, pentane (−28 °C, 15 mL) was added, and the mixture allowed to stand at −28 °C for 1 h. The solids were isolated by filtration, washed with pentane (−28 °C, 2 × 2 mL), and dried briefly to afford the respective phosphine complexes. The ^{13}CO derivatives [**1d′**]BF_4 and [**1e′**]BF_4 were prepared analogously using [(dppe)Ni(pdt)Fe($^{13}CO)_3$][9] as the precursor.

*[(dppe)Ni(pdt)Fe$(CO)_2$PHCy$_2$]BF_4 ([**1a**]BF_4).* Yield: 74%, brown powder. ESI-MS: m/z 872.3 ([M − BF_4^-]$^+$). Anal. Calcd for $C_{43}H_{53}BF_4FeNiO_2P_3S_2\cdot0.25CH_2Cl_2$: C, 52.93; H, 5.49; N, 0.00. Found: C, 52.77; H, 5.52; N, 0.00.

*[(dppe)Ni(pdt)Fe$(CO)_2$PPh(NEt$_2$)$_2$]BF_4 ([**1b**]BF_4).* Yield: 69%, olive powder. ESI-MS: m/z 926.1 ([M − BF_4^-]$^+$). Anal. Calcd for $C_{45}H_{55}BF_4FeNiN_2O_2P_3S_2\cdot0.5CH_2Cl_2$: C, 51.71; H, 5.34; N, 2.65. Found: C, 51.79; H, 5.39; N, 2.68.

*[(dppe)Ni(pdt)Fe$(CO)_2$P(NMe$_2$)$_3$]BF_4 ([**1c**]BF_4).* Yield: 66%, olive powder. ESI-MS: m/z 836.8 ([M − BF_4^-]$^+$). Anal. Calcd for $C_{37}H_{48}BF_4FeN_3NiO_2P_3S_2\cdot0.67CH_2Cl_2$: C, 46.07; H, 5.06; N, 4.28. Found: C, 46.17; H, 5.01; N, 4.49.

*[(dppe)Ni(pdt)Fe$(CO)_2$P(^{i}Pr)$_3$]BF_4 ([**1d**]BF_4).* Yield: 75%, olive powder. ESI-MS: m/z 834.1 ([M − BF_4^-]$^+$), 806.2 ([M − CO − BF_4^-]$^+$). Anal. Calcd for $C_{40}H_{51}BF_4FeNiO_2P_3S_2$: C, 52.09; H, 5.57; N, 0.00. Found: C, 51.65; H, 5.72; N, 0.10.

*[(dppe)Ni(pdt)Fe($^{13}CO)_2$P(^{i}Pr)$_3$]BF_4 ([**1d′**]BF_4).* Yield: 70%, olive powder. ESI-MS: m/z 836.3 ([M − BF_4^-]$^+$). Anal. Calcd for $C_{38}{}^{13}C_2H_{51}BF_4FeNiO_2P_3S_2\cdot0.25CH_2Cl_2$: C, 51.13; H, 5.49; N, 0.00. Found: C, 51.16; H, 5.59; N, 0.00.

*[(dppe)Ni(pdt)Fe$(CO)_2$PCy$_3$]BF_4 ([**1e**]BF_4).* Yield: 94%, green powder. ESI-MS: m/z 954.3 ([M − BF_4^-]$^+$), 926.4 ([M − CO − BF_4^-]$^+$). Anal. Calcd for $C_{49}H_{63}BF_4FeNiO_2P_3S_2\cdot0.67CH_2Cl_2$: C, 54.27; H, 5.90; N, 0.00. Found: C, 54.49; H, 6.14; N, 0.26.

Green hexagonal single crystals were grown by layering a concentrated CH_2Cl_2 solution with pentane and allowing the mixture to stand at −28 °C. One crystal (0.322 × 0.197 × 0.054 mm) was subjected to X-ray diffraction at 193 K. Its space group was determined to be trigonal $P\bar{3}$ with cell parameters a = 20.768 Å, b = 20.768 Å, c = 27.300 Å, α = 90°, β = 90°, and γ = 120°. Integration of 5773 reflections and solution by direct methods using *SHELXTL V6.12*[38,39] afforded a model with R1 = 0.0631 and wR2 = 0.1684.

*[(dppe)Ni(pdt)Fe($^{13}CO)_2$PCy$_3$]BF_4 ([**1e′**]BF_4).* Yield: 73%, green powder. ESI-MS: m/z 956.2 ([M − BF_4^-]$^+$), 673.3 ([M − ^{13}CO − PCy_3 − BF_4^-]$^+$). Anal. Calcd for $C_{49}{}^{13}C_2H_{63}BF_4FeNiO_2P_3S_2\cdot0.75CH_2Cl_2$: C, 53.92; H, 5.87; N, 0.00. Found: C, 53.93; H, 5.88; N, 0.00.

*[(dcpe)Ni(pdt)Fe$(CO)_2$PPh$_2$(2-py)]BF_4 ([**2a**]BF_4).* Yield: 80%, yellow powder. ESI-MS: m/z 961.3 ([M − BF_4^-]$^+$), 933.3 ([M − CO − BF_4^-]$^+$). Anal. Calcd for $C_{48}H_{68}BF_4FeNNiO_2P_3S_2\cdot0.25CH_2Cl_2$: C, 47.38; H, 6.45; N, 1.31. Found: C, 54.18; H, 6.12; N, 1.36.

*[(dcpe)Ni(pdt)Fe$(CO)_2$PPh$_3$]BF_4 ([**2b**]BF_4).* Yield: 79%, yellow powder. ESI-MS: m/z 960.8 ([M − BF_4^-]$^+$). Anal. Calcd for $C_{49}H_{69}BF_4FeNiO_2P_3S_2\cdot3.25CH_2Cl_2$: C, 47.38; H, 5.75; N, 0.00. Found: C, 47.43; H, 5.87; N, 0.00.

*[(dcpe)Ni(pdt)Fe$(CO)_2$PCy$_3$]BF_4 ([**2c**]BF_4).* Yield: 62%, green powder. ESI-MS: m/z 978.2 ([M − BF_4^-]$^+$), 950.2 ([M − CO − BF_4^-]$^+$), 670.2 ([M − PCy_3 − CO − BF_4^-]$^+$). Anal. Calcd for $C_{49}H_{87}BF_4FeNiO_2P_3S_2\cdot2.5CH_2Cl_2$: C, 48.36; H, 7.25; N, 0.00. Found: C, 48.19; H, 7.30; N, 0.00.

Green prismatic single crystals of [**2c**]$BF_4\cdot CH_2Cl_2\cdot$0.5pentane were grown by layering a concentrated CH_2Cl_2 solution with pentane and allowing the mixture to stand at −28 °C. One crystal (0.514 × 0.133 × 0.042 mm) was subjected to X-ray diffraction at 193 K. Its space group was determined to be monoclinic $P2_1/n$ with cell parameters a = 21.873 Å, b = 10.784 Å, c = 26.362 Å, α = 90°, β = 107.63°, and γ = 90°. Integration of 3186 reflections and solution by direct methods using *SHELXTL V6.12*[38,39] afforded a model with R1 = 0.1217 and wR2 = 0.2317.

CALCULATIONS

Calculations of the structural parameters and the electronic structure were performed using *ORCA*.[40] Full geometry optimizations were performed using the B3LYP[41] and BP86[42,43] exchange-correlation functionals and a triple-ζ basis set with polarization functions that were obtained from the

dx.doi.org/10.1021/ic300910r | Inorg. Chem. 2012, 51, 8931−8941

TURBOMOLE library.[44] This combination of the exchange-correlation functional and basis set was shown to give accurate structural parameters. In addition, single-point calculations using the hybrid B3LYP[41] and PBE0[45,46] functionals were carried out on the BP86/TZVP geometry-optimized structures. In order to incorporate van der Waals interactions, a simple semi-empirical correction scheme was used to account for the major parts of this contribution.[47] IR spectra were generated by numerically calculating second derivatives; calculations of **g** tensors were performed using an effective mean-field spin–orbit coupling operator, with the center of mass as the origin of the **g** tensor.[48] Additional **g**- and **A**-tensor calculations were performed with ADF[49,50] using ZORA[51] for relativistic effects and a self-consistent inclusion of the spin–orbit coupling. A Slater-orbital DZ basis set was used for spin-restricted **g**-tensor calculations[52] and a TZP basis set for spin-unrestricted scalar relativistic hyperfine coupling tensor calculations.[53,54]

■ ASSOCIATED CONTENT

Supporting Information

X-ray crystallographic data in CIF format, cyclic voltammograms, positive-ion ESI-MS, FT-IR, X- and Q-band EPR, and UV–vis spectra, schematic drawing of $[1e]^{+a}$, bond distances and angles, atomic spin populations, and calculated **g**-tensor principal values. This material is available free of charge via the Internet at http://pubs.acs.org.

■ AUTHOR INFORMATION

Corresponding Author

*E-mail: rauchfuz@illinois.edu (T.B.R.), matthias.stein@mpi-magdeburg.mpg.de (M.S.).

Notes

The authors declare no competing financial interest.

■ ACKNOWLEDGMENTS

The authors thank Drs. Danielle L. Gray and Amy L. Fuller for X-ray crystallography and Dr. Mark J. Nilges for assistance with EPR spectroscopy. This work was supported by the National Institutes of Health (Grant GM46441) and the Max Planck Society.

■ REFERENCES

(1) Frey, M. *ChemBioChem* **2002**, *3*, 153.
(2) Shima, S.; Pilak, O.; Vogt, S.; Schick, M.; Stagni, M. S.; Meyer-Klaucke, W.; Warkentin, E.; Thauer, R. K.; Ermler, U. *Science* **2008**, *321*, 572.
(3) Vignais, P. M.; Billoud, B. *Chem. Rev.* **2007**, *107*, 4206.
(4) Peters, J. W.; Lanzilotta, W. N.; Lemon, B. J.; Seefeldt, L. C. *Science* **1998**, *282*, 1853.
(5) Nicolet, Y.; Piras, C.; Legrand, P.; Hatchikian, C. E.; Fontecilla-Camps, J. C. *Structure* **1999**, *7*, 13.
(6) Siegbahn, P. E. M.; Tye, J. W.; Hall, M. B. *Chem. Rev.* **2007**, *107*, 4414.
(7) Stiebritz, M. T.; Reiher, M. *Inorg. Chem.* **2010**, *49*, 5818.
(8) Fichtner, C.; van Gastel, M.; Lubitz, W. *Phys. Chem. Chem. Phys.* **2003**, *5*, 5507.
(9) Schilter, D.; Nilges, M. J.; Chakrabarti, M.; Lindahl, P. A.; Rauchfuss, T. B.; Stein, M. *Inorg. Chem.* **2012**, *51*, 2338.
(10) Hatchikian, E. C.; Bruschi, M.; Le Gall, J. *Biochem. Biophys. Res. Commun.* **1978**, *82*, 451.
(11) Ogata, H.; Lubitz, W.; Higuchi, Y. *Dalton Trans.* **2009**, 7577.
(12) De Lacey, A. L.; Fernández, V. M.; Rousset, M.; Cammack, R. *Chem. Rev.* **2007**, *107*, 4304.
(13) Stein, M.; Lubitz, W. *Phys. Chem. Chem. Phys.* **2001**, *3*, 5115.
(14) Camara, J. M.; Rauchfuss, T. B. *Nat. Chem.* **2011**, *4*, 26.
(15) De Lacey, A. L.; Stadler, C.; Fernandez, V. M.; Hatchikian, E. C.; Fan, H. J.; Li, S. H.; Hall, M. B. *J. Biol. Inorg. Chem.* **2002**, *7*, 318.
(16) (a) Tard, C.; Pickett, C. J. *Chem. Rev.* **2009**, *109*, 2245. (b) Ohki, Y.; Tatsumi, K. *Eur. J. Inorg. Chem.* **2011**, 973.
(17) Barton, B. E.; Olsen, M. T.; Rauchfuss, T. B. *J. Am. Chem. Soc.* **2008**, *130*, 16834.
(18) Liu, T.; Darensbourg, M. Y. *J. Am. Chem. Soc.* **2007**, *129*, 7008.
(19) Foerster, S.; Stein, M.; Brecht, M.; Ogata, H.; Higuchi, Y.; Lubitz, W. *J. Am. Chem. Soc.* **2003**, *125*, 83.
(20) Bennett, B.; Lemon, B. J.; Peters, J. W. *Biochemistry* **2000**, *39*, 7455.
(21) Justice, A. K.; Gioia, L. D.; Nilges, M. J.; Rauchfuss, T. B.; Wilson, S. R.; Zampella, G. *Inorg. Chem.* **2008**, *47*, 7405.
(22) Rahman, M. M.; Liu, H.-Y.; Eriks, K.; Prock, A.; Giering, W. P. *Organometallics* **1989**, *8*, 1.
(23) Crabtree, R. H.; Lavin, M. *Inorg. Chem.* **1986**, *25*, 805.
(24) Barton, B. E.; Rauchfuss, T. B. *J. Am. Chem. Soc.* **2010**, *132*, 14877.
(25) Addison, A. W.; Rao, T. N.; Reedijk, J.; van Rijn, J.; Verschoor, G. C. *J. Chem. Soc., Dalton Trans.* **1984**, 1349.
(26) Cordero, B.; Gómez, V.; Platero-Prats, A. E.; Revés, M.; Echeverría, J.; Cremades, E.; Barragán, F.; Alvarez, S. *Dalton Trans.* **2008**, 2832.
(27) Higuchi, Y.; Ogata, H.; Miki, K.; Yasuoka, N.; Yagi, T. *Structure* **1999**, *7*, 549.
(28) Peters, J. W.; Lanzilotta, W. N.; Lemon, B. J.; Seefeldt, L. C. *Science* **1998**, *282*, 1853.
(29) Carroll, M. E.; Barton, B. E.; Gray, D. L.; Mack, A. E.; Rauchfuss, T. B. *Inorg. Chem.* **2011**, *50*, 9554.
(30) Sowa, J. R.; Zanotti, V.; Facchin, G.; Angelici, R. J. *J. Am. Chem. Soc.* **1992**, *114*, 160.
(31) Barton, D. H. R.; Jang, D. O.; Jaszberenyi, J. C. *Tetrahedron* **1993**, *49*, 7193.
(32) Ogata, H.; Mizoguchi, Y.; Mizuno, N.; Miki, K.; Adachi, S.-i.; Yasuoka, N.; Yagi, T.; Yamauchi, O.; Hirota, S.; Higuchi, Y. *J. Am. Chem. Soc.* **2002**, *124*, 11628.
(33) Bunten, K. A.; Chen, L.; Fernandez, A. L.; Poë, A. J. *Coord. Chem. Rev.* **2002**, *233–234*, 41.
(34) Thomas, C. M.; Darensbourg, M. Y.; Hall, M. B. *J. Inorg. Biochem.* **2007**, *101*, 1752.
(35) Jiang, J.; Maruani, M.; Solaimanzadeh, J.; Lo, W.; Koch, S. A.; Millar, M. *Inorg. Chem.* **2009**, *48*, 6359.
(36) Ohki, Y.; Yasumura, K.; Ando, M.; Shimokata, S.; Tatsumi, K. *Proc. Natl. Acad. Sci. U.S.A.* **2010**, *107*, 3994.
(37) Bras, J. L.; Jiao, H.; Meyer, W. E.; Hampel, F.; Gladysz, J. A. *J. Organomet. Chem.* **2000**, *616*, 54.
(38) Sheldrick, G. M. *Acta Crystallogr.* **2008**, *A64*, 112.
(39) *SHELXTL*; Bruker AXS, Inc.: Madison, WI.
(40) Neese, F. *ORCA—An ab initio, DFT and semiempirical SCF-MO package*, version 2.8.0; University of Bonn, Bonn, Germany.
(41) Becke, A. D. *J. Chem. Phys.* **1993**, *98*, 5648–5652. Lee, C.; Yang, W.; Parr, R. G. *Phys. Rev. B* **1988**, *37*, 785–789. Vosko, S. H.; Wilk, L.; Nusair, M. *Can. J. Phys.* **1980**, *58*, 1200–1211. Stephens, P. J.; Devlin, F. J.; Chabalowski, C. F.; Frisch, M. J. *J. Phys. Chem.* **1994**, *98*, 11623–11627.
(42) Becke, A. D. *Phys. Rev. A* **1988**, *38*, 3098.
(43) Perdew, J. P. *Phys. Rev. B* **1986**, *33*, 8822.
(44) Schaefer, A.; Huber, C.; Ahlrichs, R. *J. Chem. Phys.* **1994**, *100*, 5829. Also ftp.chemie.uni-karlsruhe.de/pub/basen.
(45) Ernzerhof, M.; Scuseria, G. *J. Chem. Phys.* **1999**, *110*, 5029.
(46) Adamo, C.; Barone, V. *J. Chem. Phys.* **1999**, *110*, 6158.
(47) Grimme, S. *J. Comp. Chem.* **1787**, *27*, 1787.
(48) Neese, F. *J. Chem. Phys.* **2001**, *115*, 11080. Neese, F. *J. Chem. Phys.* **2005**, *122*, 034107.
(49) te Velde, G.; Bickelhaupt, F. M.; van Gisbergen, S. J. A.; Guerra, C. F.; Baerends, E. J.; Snijders, J. G.; Ziegler, T. *J. Comput. Chem.* **2001**, *22*, 931.

(50) *ADF2010*; SCM, Theoretical Chemistry, Vrije Universiteit: Amsterdam, The Netherlands.
(51) van Lenthe, E.; Baerends, E. J.; Snijders, J. G. *J. Chem. Phys.* **1993**, *99*, 4597.
(52) van Lenthe, E.; van der Avoird, A.; Wormer, P. E. S. *J. Phys. Chem.* **1997**, *107*, 2488.
(53) van Lenthe, E.; van der Avoird, A.; Wormer, P. E. S. *J. Chem. Phys.* **1998**, *108*, 4783.
(54) van Lenthe, E.; Baerends, E. J. *J. Chem. Phys.* **2000**, *112*, 8279.

■ NOTE ADDED AFTER ASAP PUBLICATION

This paper was published on the Web on July 27, 2012, with the incorrect information for reference 48. The corrected version was reposted on August 3, 2012.